Journal of the Mechanical Behavior of Biomedical Materials 118 (2021) 104461

Contents lists available at ScienceDirect

Journal of the Mechanical Behavior of Biomedical Materials

journal homepage: http://www.elsevier.com/locate/jmbbm

Titanium mesh-reinforced calcium sulfate for structural bone grafts

S. Cavelier [a], S.A. Mirmohammadi [a], F. Barthelat [a,b,*]

[a] Department of Mechanical Engineering, McGill University, Montreal, Quebec, Canada
[b] Department of Mechanical Engineering, University of Colorado, Boulder CO, USA

ARTICLE INFO

Keywords:
Fracture
Multi-layer
Composite
Bone graft
Optimization

ABSTRACT

Calcium sulfate (CS) possesses many of the requirements for an ideal bone graft material: it is biodegradable, biocompatible, and osteoconductive. However, its relatively low strength and brittleness are major obstacles to its use as a structural bone implant. Although the strength of CS can be improved by reducing porosity, its brittleness remains a major obstacle towards its use as bone graft. Here we combine two powerful toughening strategies which are found in advanced ceramics and in natural bone: Multi-layered architectures and ductile reinforcements. We first used stress analysis and micromechanics to generate design guidelines that ensure the proper failure sequence and maximize properties. We then fabricated and tested fully dense CS by hydrostatic compression layered with layers of titanium woven mesh. Flexural experiments in hydrated conditions confirmed that the ductility and strength of titanium and the adhesion at the titanium-CS interfaces (controlled by the size of the Ti mesh) are critical factors in the mechanical performance of the composite. Our best design exhibited a toughness 180 times larger than that of plain CS, together with a 46% increase in strength.

1. Introduction

Large segmental bone defects are the consequence of various diseases such as highly complex traumatic and post-traumatic injuries, bone tumors, or infections. Millions of patients worldwide suffer from large segmental bone defects (Bohner et al., 2012; Hall et al., 2010) and orthopedic surgery fails to provide fully adequate treatment options, with failure rates approaching 25% (Mankin, 1987). The study of the first allograft surgery attempts on humans in the late 19th Century by Vittorio Putti (Donati et al., 2007) led to a better understanding of bone healing and of the principles of bone grafting science that still apply today. Among these, Putti noted the importance of asepsis, of the mechanical characteristics of the graft and the surrounding tissues, and of the role of the osteogenetic capability of the graft in its integration. Based on a century of bone grafting history, Bohner (Bohner et al., 2012) later extended Putti's principles to three major requirements to be fulfilled for an ideal bone graft: (i) mechanical properties that match healthy bone in terms of stiffness, strength, and toughness; (ii) biocompatibility, osteoinductivity, and osteoconductivity to promote healing and bone cell recruitment; (iii) ability to degrade and resorb at a rate similar to healthy bone. Modern techniques enabled autografting and xenografting procedures despite the associated complications such as viral and bacterial transmission (Zamborsky et al., 2016), immunological incompatibility (Bohner, 2010), and non-union or structural failure (Muller et al., 2013). The discovery of biocompatible materials accelerated the development of available grafting techniques. A popular biomaterial is titanium (Ti), which is biocompatible and strong, but this metal is much stiffer than bone (leading to stress shielding (Noyama et al., 2012)) and does not resorb (Hahn and Palich, 1970). Polymers such as polylactic acid, polyglycolic acid, or collagen-derived biomaterials offer interesting properties in terms of biocompatibility and resorption, but they have poor structural integrity (Coombes and Meikle, 1994; Pneumaticos et al., 2010). Bioceramics or bioglass ceramics are fully or partially biodegradable and relatively stiff, but they have low fracture toughness and cannot reliably carry skeletal forces (Saini et al., 2015; Moore et al., 2001). Finally, biocompatible minerals such as hydroxyapatite (HA), calcium sulfate (CS), or calcium phosphate (CP) offer a compromise among degradability, osteoconductivity, and mechanical properties because of their chemical composition (Bohner et al., 2012; Turner et al., 2003; Maeda et al., 2007; Baino et al., 2017). However they present disadvantages for bone grafting purposes: CP resorbs at a faster rate than bone growth (Moore et al., 2001), it is not osteoinductive, and it does not match the mechanical properties of natural bone (LeGeros, 2002); HA resorbs too slowly over years (Bohner et al., 2012; Moore et al., 2001; Ranjan, 2010), and CS does not approach the mechanical properties of bone

* Corresponding author. Department of Mechanical Engineering, University of Colorado, Boulder CO, USA.
E-mail address: francois.barthelat@colorado.edu (F. Barthelat).

https://doi.org/10.1016/j.jmbbm.2021.104461
Received 12 September 2019; Received in revised form 10 March 2021; Accepted 11 March 2021
Available online 18 March 2021

(Anusavice, 2003) despite its promising bone regeneration capability (Coetzee, 1980; McKee and Bailey, 1984). In the absence of in-vivo structural integrity, CS is therefore primarily used for non-load bearing grafts or as defect-filling granulates (Moore et al., 2001; Pietrzak and Ronk, 2000). In previous work (Cavelier et al., 2020), the authors have addressed the problem of the low strength of CS and have optimized CS fabrication parameters. The most relevant improvement in strength was obtained by reducing the porosity of the material from 54% to less than 2% by compressing the powder-water slurry during its setting phase. Flexural strength dramatically increased from 12 to 31.8 MPa, but the addition of inclusions (glass fibres, mineral or ceramic whiskers, microtablets, and beads) did not improve the mechanical properties of the porosity-reduced CS.

Optimized CS is still brittle, and its mechanical behavior is far from that of natural bone. The remarkable performance of bone is due partly to its structure, which consists of seven hierarchical levels. Each level has its own energy-dissipation and toughening mechanisms (Weiner and Wagner, 1998), uncracked-ligament bridging being the most predominant (Nalla et al., 2003, 2004, 2005). Interfaces are present at most of the hierarchical levels and play an important role in deflecting incoming cracks (Ager et al., 2006; Koester et al., 2008). Non-collagenous proteins such as osteopontin accumulate in these interfaces and are also essential for the overall toughness of bone (Thurner et al., 2010). The recent measurements of the adhesive properties of crosslinked osteopontin suggest that energy is dissipated through sacrificial bonds (Cavelier et al., 2018). This combination of micro-architecture, interfaces and adhesive provides a major contribution to the overall toughness of bone (Ritchie et al., 2009). The toughening mechanisms related to the presence of interfaces between dissimilar materials exist not only in bone, but also in other mineralized natural materials such as nacre (Barthelat et al., 2007) or enamel (Zhang et al., 2014; Bechtle et al., 2010), which are among the most mechanically efficient natural materials (Ritchie et al., 2009; Barthelat and Rabiei, 2011). These observations suggest that designing weak interfaces in brittle ceramics is a strategy to toughen them. Clegg (Clegg et al., 1990) successfully increased the toughness of brittle silicon carbide by multi-layering its architecture with weak interfaces. Unlike bulk ceramic, where cracks propagated through the material, with the direct effect of increasing the stress intensity factor at the crack tip, incoming cracks were deflected along the interfaces, parallel with the applied stress, so that the stress intensity factor decreased, leading to a more stable fracture (Clegg, 1992; Phillipps et al., 1993). This delay in complete failure dissipated 160 times more energy and required more loading than bulk silicon carbide. The strength of the ceramic was improved, and even more dramatically, its toughness. Kovar et al. (1998) demonstrated that interfaces with lower toughness or lower stiffness than the layers were more likely to deflect cracks and increase the overall toughness of the material. Analytical models from He and Hutchinson (He et al., 1994) indicated that the energy criterion to ensure crack deflection was $\frac{\Gamma_i}{\Gamma_l} < \frac{1}{4}$, where Γ_i is the toughness of the interface and Γ_l the toughness of the layer. Paradoxically, this criterion pointed to the importance of softer interfaces to initiate toughening mechanisms and increase the overall toughness of a multi-layered beam.

Another strategy to reinforce brittle ceramics is to use a ductile phase (Krstic, 1983; Sigl et al., 1988). Ductile particles that are perpendicular to crack propagation can store energy while stretched in the crack wake. The associated tensioning forces limit crack propagation, a phenomenon called crack bridging that increases the strain of the composite (strain hardening) and its work-of-fracture (or toughness). Ductile fibres are efficient for reinforcing brittle ceramics. Not only do they contribute to toughness by plastic dissipation during crack bridging (Evans, 1990), but they also provoke many other toughening mechanisms: debonding toughness of the matrix-fibre interface (Evans, 1990; Campbell et al., 1990) and crack deflection along the fibre-matrix weak interfaces are important contributors to toughness. They also delay fracture of the fibres. In addition, fibres that fail in the matrix are subjected to pull-out, which dissipates energy by frictional slipping (Thouless and Evans, 1988). This strategy has been used successfully on biocompatible cements. For instance, the work-of-fracture of CP has been increased with chitosan-PLGA fibres or polycaprolactone (Kruger and Groll, 2012), with collagen (Moreau et al., 2009), and 100 times with polyglactin fibres (Xu and Quinn, 2002). A similar trend was observed on CS with cellulose fibres (Coutts, 1986). Finally, Ti fibres improved the fracture toughness of bone cement by 56% (Topoleski et al., 1992). The simultaneous existence of several mechanisms is of interest because the overall toughness of the composite can be superior to the sum of the contributions (Evans, 1990). Investigations of the optimization of these mechanisms are therefore critical. Low ceramic-fibre interface toughness is necessary to promote fibre pull-out, surface debonding, and crack deflection (Campbell et al., 1990; Budiansky et al., 1986) to reduce stress singularities, and to delay fibres fracture (Evans and McMeeking, 1986). The length of the fibres (Li et al., 1991) and their alignment (Campbell et al., 1990) are two other critical parameters in optimizing the design. From this point of view, fibres interlaced in patterns, or textiles, provide more control of the architecture of the reinforced matrix and promote the same toughening mechanisms as observed with fibres reinforced ceramics. This strategy is used in bullet-proof armor, where the woven aramid mesh gives the composite the ability to dissipate high energy (Kyung and Meyer, 2006). A biocompatible ceramic reinforced with plain-weave glass textile also demonstrated that biocompatibility, osteointegration, and superior mechanical properties (strength and stiffness) could be combined with this strategy (Suchy et al., 2008).

The present work addresses the problem of the brittleness of CS by combining CS with a ductile material (interlayer) into a multi-layered architecture to approach the strength (150 MPa (Weiner and Wagner, 1998)) and toughness (3–10 MPa m$^{1/2}$ (Ritchie et al., 2009)) of natural bone. First, analytical and numerical models are presented to predict the effect of geometrical and mechanical parameters on mechanical performance. Then a fabrication protocol is proposed for a CS-Ti mesh multi-layered composite. The effects of mesh geometry, the number of layers, and the Ti volume fraction on the mechanical properties of the composite are investigated.

1.1. Stress analysis and failure

For the ductile interlayers to efficiently reinforce the brittle layers, it is critical to ensure that failure occurs in the proper sequence. In uniaxial tension along the layers and under uniform strain conditions, the brittle layers will start fracturing first, while the more ductile interlayers can hold fragments together and increase toughness. Under flexural loading representative of bone graft materials however, this failure mode does not automatically occur because the stresses are not uniform. In this section we present a simple model that can guide the design of the material to ensure that the ductile interlayers provide a sustained reinforcement in flexural mode. Fig. 1 is a schematic view of the material design. We consider a beam (total thickness t, width b, span L) composed of N layers of a stiff but brittle material (index ‘l’ for layer, thickness = t_l)

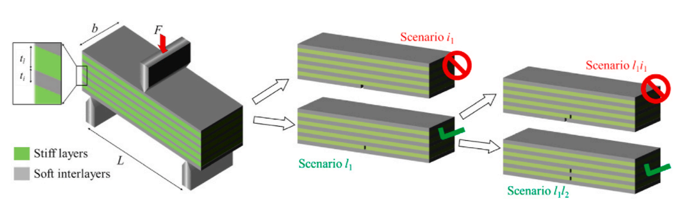

Fig. 1. Overview of the multi-layered beam modeled in this section and its geometrical and mechanical characteristics. The analytical model predicts whether scenario l_1 or i_1 occurs. Finite-element analysis assumes a debonding length d in scenario l_1 and predicts whether scenario $l_1 l_2$ or $l_1 i_1$ occurs.

reinforced by N+1 ductile interlayers (index 'i' for interlayer, thickness $= t_i$). The volume fraction of the stiff material is therefore written:

$$\varphi = \frac{Nt_l}{t} \tag{1}$$

The relevant mechanical properties are the Young's modulus and tensile strength for the stiff material (E_l and S_l) and the Young's modulus and yield strength for the ductile interlayer material (E_i and S_i). Because the role of the interlayer material is to strengthen the composite, we assume that $S_i > S_l$. Individual layers of hard material are labelled l_k (k = 1: lowermost layer) and the softer interlayers are labelled i_k (k = 1: lowermost interlayer). The beam is subjected to a transverse force F (Fig. 1), which may lead to several possible failure scenarios which we examine next. Since the tensile stresses are the highest near the surface of the beam, the first failure may occur at the lowermost interlayer (scenario i_1 on Fig. 1). Since the interlayers must act as reinforcements for the more brittle layers, this scenario is not desired. A second, more favorable first failure mode occurs at the lowermost hard layer while the lowermost interlayer remains intact (scenario l_1 on Fig. 1). Following this first failure of the brittle layer, a possible scenario l_1i_1 (Fig. 1) involves the failure of the outer ductile interlayer. This scenario is not desirable, because it prevents the reinforcement from these layers. A more favorable failure is where the next hard layer fails (scenario l_1l_2). The objective of the models is to predict the conditions for scenario l_1l_2 to prevail, which will guide the selection of an optimal reinforcing material for the interlayer and suggest optimal architecture.

A stress analysis on the beam, detailed in the appendix, produces the following condition for failure scenario l_1 to prevail:

$$\frac{S_i E_l}{S_l E_i}\left(1 - 2\frac{1-\varphi}{N+1}\right) > 1 \tag{2}$$

From this result we constructed a failure map as a function of the ratio of the strength of the hard layer to that of the interlayer and the ratio of the stiffness of these materials (Fig. 2a, φ and N fixed). The map highlights how scenario l_1 is promoted by low relative Young's modulus E_i/E_l (low modulus for the interlayers and/or high modulus for the hard layer) and high relative strength (high strength for the interlayers and/or low strength for the hard layer). Fig. 2b highlights the effects of hard material concentration φ and number of layers N (E_i/E_l fixed). A large number of layers and a high volume fraction of the hard layers both promote scenario l_1.

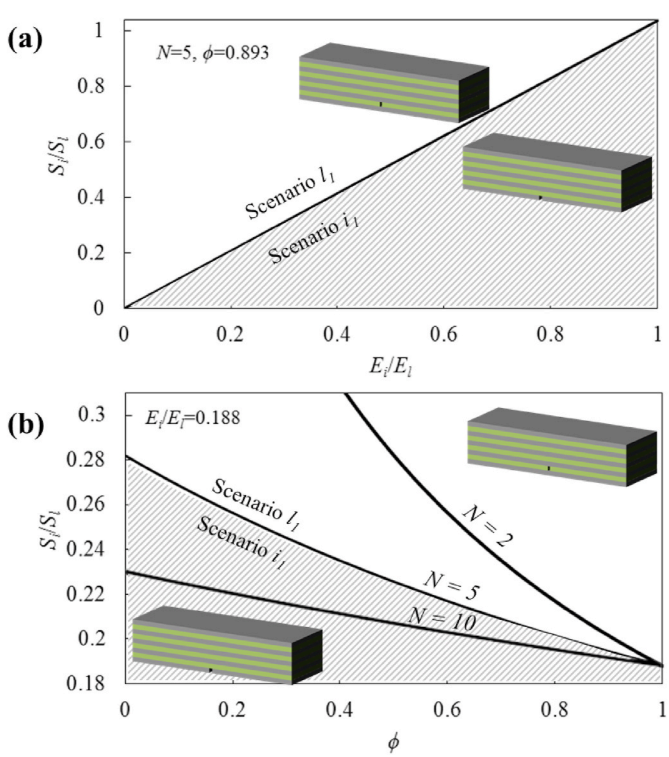

Fig. 2. a) Effect of the elastic modulus ratio and the strength ratio on the failure of the interlayer or the CS layer; b) effect of the number of layers, volume fraction, and strength ratio on the failure of the interlayer or the CS layer.

We now examine the possible failure scenario once l_1 had occurred. Assuming that the lowermost hard layer has fractured, an edge crack is present in the system. If the other layers and interlayers are intact, the high stresses at the tip of the crack must be absorbed by the delamination of the layer (Clegg, 1992; Phillipps et al., 1993; Chan et al., 1993) over a distance d (Fig. 3). This configuration makes stress analysis more complicated, and therefore we examined the problem using the finite element method. We built finite element models using ANSYS Parametric Design Language (APDL) to automatically generate a wide range of architectures with various debonded lengths d (Fig. 3b). More details of the finite-element model can be found in the Appendix. The debonded length d can take small values, or very large values that may completely "split" the beam. The extent of delamination d can be controlled by the toughness of the interface between the layer and the interlayer, but we did no try to explicitly capture delamination in the simulations. Instead, we performed a series of stress analyses on systems with various lengths d. We hypothesised that d has an optimum value large enough to redistribute stresses in the adjacent layers, yet small enough to prevent complete delamination.

Once the state of stress is known for a given architecture, delamination length and materials properties, we applied a stress-based criterion to predict whether failure would occur in the soft interlayers (scenario l_1i_1, Fig. 1) or in the next hard layer (scenario l_1l_2). The objective of the model was to predict the conditions for desired scenario l_1l_2 to prevail. Fig. 4 shows typical failure maps obtained from the stress analysis as function of the delamination length d and the strength ratio for various modulus ratios (Fig. 4a) and number of layers (Fig. 4b). In general, scenario l_1l_2 is promoted for strong but soft interlayers (high S_i/S_l, low E_i/E_l) and a large number of layers N. The effect of the debonding length is more complex. Scenario l_1l_2 is promoted by either very short ($d/t_l < 0.1$) or very large debonded lengths ($d/t_l > 3$). Since debonding cannot be avoided in the actual material, it is easier in terms of design and material control to aim for long debonded lengths. However, if the interface must be weak enough for long debonded length, it must also be strong enough to prevent catastrophic delamination. For example, preliminary results on CS beams multi-layered with continuous metallic foils resulted in materials that easily split along the very weak metal-CS interfaces. These results and observations suggest the presence of an optimum value for the adhesion between the hard layers and the interlayers.

Taking into account the design guidelines indicated by the analytical and numerical models, a composite with ductile interlayers, optimal

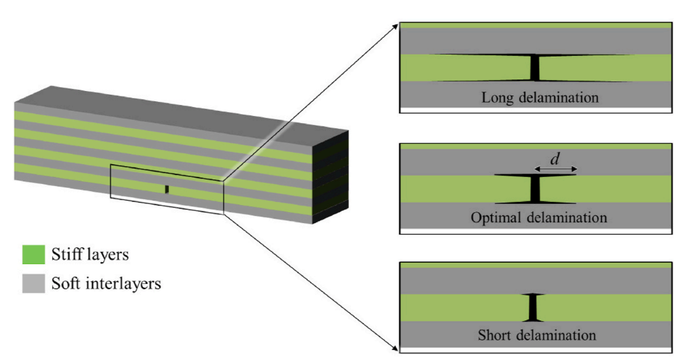

Fig. 3. Once the lowermost stiff layer has fractured, high stresses at the tip can induce delamination over a distance d.

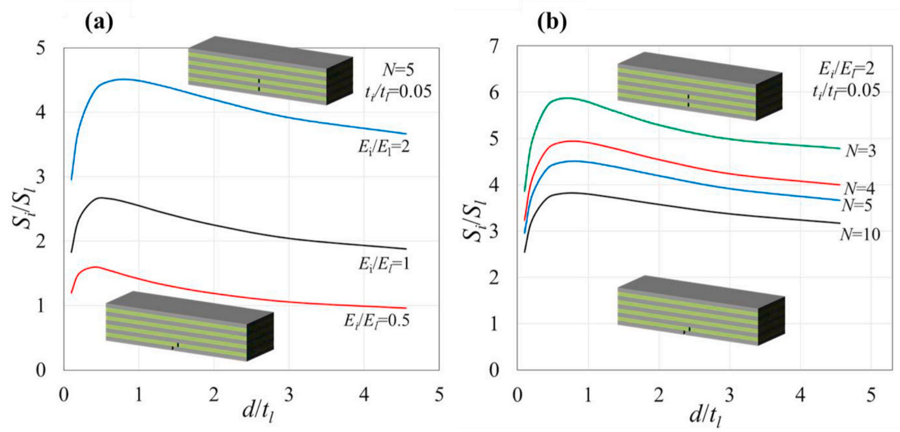

Fig. 4. Fracture maps indicating the occurrence of the l_1l_2 or l_1i_1 scenario as function of a) debonding length and elastic modulus ratio; b) debonding length and number of bilayers.

layer-interlayer adhesion that enables non-catastrophic delamination, and a large number of layers will promote the l_1l_2 scenario. Fig. 5 displays a strength-modulus chart for a large number of biocompatible artificial and natural materials. We assumed that the properties of the hard material are fixed: fully dense calcium sulfate (CS) with $S_l = 31$ MPa and $E_l = 11$ GPa, chosen for its relatively high modulus and biocompatibility. We then used the three design guidelines to select materials of interest for the interlayers. First we used equation (2) with $N = 5$ and $\varphi = 0.893$ (which are typical of the materials we fabricated), $S_l = 31$ MPa and $E_l = 11$ GPa. This provided the condition $\frac{S_i}{E_i} > 2.92$ on the interlayers to ensure that scenario l_1 initially prevails. This condition excludes materials like glasses and ceramics for the interfaces. The second design guideline was based on maximizing S_i/S_l and minimizing E_i/E_l. Since S_l and E_l are fixed, the second design guideline translates into finding interlayer materials that maximize $\frac{S_i}{E_i}$. Finally, the third guideline we used relates to energy dissipation in tension. Since crack bridging by ductile layers is intended to be the main toughening mechanism, a material with high energy absorbing capability is desired. Energy absorption can be approximated with $U_i \sim \frac{1}{2}\frac{S_i^2}{E_i}$ and therefore we sought materials that also maximize $\frac{S_i^2}{E_i}$ (or minimize $\frac{E_i}{S_i^2}$). Considering these three guidelines, we chose titanium (Ti) for the ductile interlayers (Fig. 5). Ti satisfies $\frac{S_i}{E_i} > 2.92$ and it has a relatively high $\frac{S_i}{E_i}$ and high $\frac{S_i^2}{E_i}$. However, as mentioned above continuous Ti layers have poor adhesion on CS. Therefore we used Ti in the form of woven meshes which provided better adhesion between Ti and CS. The meshed architecture also provided another morphological parameter (mesh coarseness) that could be adjusted to manipulate the adhesion between the layers and interlayers. Typical properties for the Ti mesh are also shown on Fig. 5.

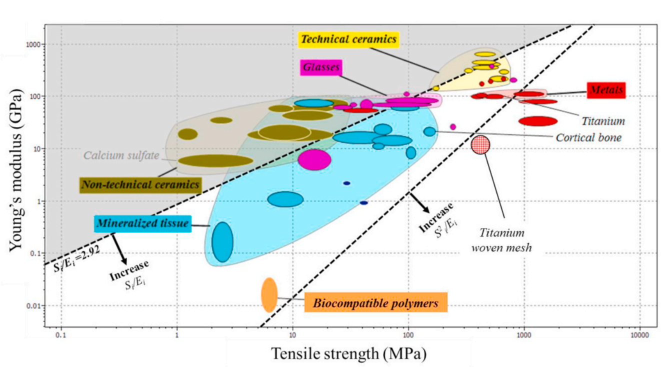

Fig. 5. Tensile strength vs. Young's modulus chart for most of the materials used in bone tissue engineering and for biogenic materials.

Ti meshes satisfy all three design guidelines for the interface choice.

2. Methods

Based on these guidelines, we propose a design and a fabrication protocol for a CS-Ti multi-layered composite. CS exists in five forms (I to V) that indicate the purity of the powder and the uniformity of the crystals (Craig and Powers, 2006). Type V is the purest form of CS and its crystals are also the most uniform in size, and as a result type V CS is the strongest with a compressive strength of 90 MPa (Azer et al., 2008). Typical preparation involves CS hemihydrate that reacts with water to form CS dihydrate. In this study powder of hemihydrate CS type V (Suprastone, Kerr Dental, Charlotte, NC) was mixed with water at a ratio of 10 g of powder to 1.86 g of water to harden (ratio indicated by the manufacturer). In a previous study (Cavelier et al., 2020) we optimized the fabrication parameters to maximize strength, and we confirmed that this mixing ratio is optimum for strength. Additionally, we established that applying hydrostatic pressure during the CS setting phase decreases porosity and improves strength. For this study we reinforced the CS layers with Ti- meshes (Wire Co., Inc. Hillside, NJ, USA) of different coarseness or open area ratios, which we defined as the surface area of the open holes divided by the total surface. We used meshes with five different open area ratios: 49%, 58%, 64%, 77%, and 88% (Fig. 6). Selecting the coarseness of the mesh can be used to tune the strength and stiffness of the mesh, as well as the adhesion of the mesh interlayer to the CS layer since larger open areas provide direct bonds between apposed CS layers and therefore higher interfacial toughness (Fig. 7d). The interlayers have different homogenized Young's moduli and strength,

Picture 10 mm			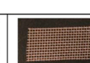	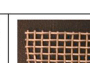	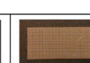
Open area (%)	88	77	64	58	49
Wire diameter (mm)	0.076	0.1	0.1	0.3	0.076
Open size (mm)	1.19	0.74	0.41	0.97	0.18
Young's modulus (GPa)	22	27	35	39	46
Strength (MPa)	25	49	81	98	123

Fig. 6. Characteristics of the five meshes used in the study, from small open area (left) to large open area (right), Homogenized strength and Young's modulus were estimated following the Voigt iso-strain model. Pictures of the Ti meshes used to fabricate the multi-layered beam are also shown.

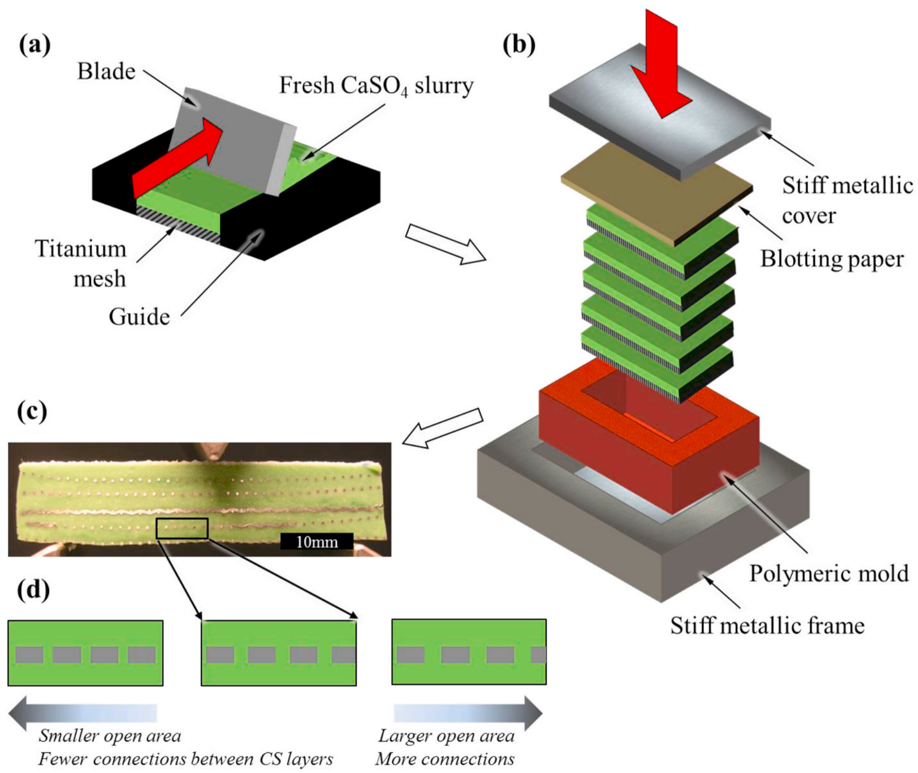

Fig. 7. a) Doctor-blading technique for uniform spreading of a fresh paste between two guides; b) assembly of five bilayers into the mold for the last step of the fabrication protocol for the multi-layered beam (hydrostatic compression); c) multi-layered beam sample (open mesh area of 58%) after setting and cutting with diamond saw; d) schematic view of three meshes with different open areas, from small (left) to large (right). Smaller open areas provide more numerous connections between the CS layers.

which we estimated using the Voigt iso-strain model and the data indicated by the manufacturer (Fig. 6). These moduli will be of interest later in the discussion of the fracture mechanisms occurring in the samples.

Because CS fully hardens only 8 min after being mixed with water, the number of bilayers (a bilayer being a single layer of CS plus a single layer of Ti-mesh) that can be fabricated at once was limited with our current method. In the fabrication protocol proposed here, all the wet bilayers must be placed under pressure together and attempts to assemble already hardened layers under pressure were unsuccessful because hardened CS is too brittle. For this reason, the number of bilayers we considered here tanged from three to seven. The analytical model also showed that a high volume fraction of CS is optimal for the mechanical performances. We therefore investigated the effect of the mesh geometry with samples with a high volume fraction of CS (94.1% vol.). Multi-layered beam samples consisting of five layers of CS and five Ti-mesh layers were prepared. CS powder was mixed with water (ratio 10:1.9) and vigorously mixed to obtain a homogeneous paste. To prepare a multi-layered sample consisting of five CS-Ti bilayers, five 30 mm by 50 mm rectangles of Ti-mesh were cut, and the freshly prepared CS paste was spread using a doctor-blading technique (Fig. 7a). Uniform thickness of the bilayers was ensured by using two tabs with controlled thickness on each side of the rectangular mesh. The thicknesses of the CS layers t_l were adjusted for each type of mesh to have a constant CS volume fraction (94.1% vol). The resulting bilayer was then placed in one of the four 30 mm by 50 mm silicone molds. These molds had a rectangular cavity with a depth of 2.5–12 mm depending on the total thickness of the sample prepared. Four additional bilayers were prepared under the same conditions and assembled inside the silicone mold within 8 min (Fig. 7b). A 40 mm by 60 mm piece of blotting paper was finally placed on top of the layers to absorb the excess water expelled from the material during compression. A pressure of 10 MPa was then applied to the structure using a 25 ton capacity hydraulic press (FW-4 tablet press, Joyfay, Cleveland, OH) to minimize porosity in the final product (Cavelier et al., 2020). This procedure resulted in samples with a fully dense and homogeneous mineral phase. Twenty-four hours after being placed in the hydraulic press, the samples were removed from their frame, and 50 mm by 7.5 mm by 2.5–11.6 mm (depending on the type of samples) beams were cut with a diamond saw (Accutom-5, Struers, Denmark). To replicate the humid conditions of the human body the samples were placed in water for about 2 h before mechanical testing (it is known that hydrated conditions decrease the strength of CS by about 25% compared to dry conditions (Cavelier et al., 2020)). The samples were tested in a three-point bending (flexure) configuration with a 40 mm span (Expert 5000, Admet, Norwood, MA) to replicate flexure in long bones.

3. Results

3.1. Effect of mesh size

We first focus on the effects of the Ti-mesh size on the flexural performance of the material. Fig. 8a shows typical flexural stress-strain curves obtained for materials reinforced with five different types of meshes. The overall thickness of each type of samples was different because the thickness of the CS layers was adjusted to maintain a constant volume fraction of CS (94.1 %vol). A minimum of three samples were tested for each mesh. Within each group of samples, the dimensions were consistent (±3.4%) and the standard deviation of the flexural strength was 10% or less. In general the stress-strain curves displayed first a linear elastic response, followed by a relatively long inelastic region with slight softening typical of fibre-reinforced cements with non-randomly distributed fibres (Yao et al., 2017). Pronounced peaks and valleys showed in this region, corresponding to the progressive cracking of the CS layers. As expected and predicted by the models, the Ti-mesh reinforcement remained unbroken in this process (Fig. 8b–f). Once every CS layer was cracked the stress dropped sharply to small values and the test was interrupted. Post mortem examination revealed that only a few wires in the Ti-mesh interlayers were fractured. Samples reinforced with Ti-mesh with open areas of 48% and 59% produced a significantly higher deformation compared to the other samples reinforced with Ti with more open mesh sizes (>60%). Pictures

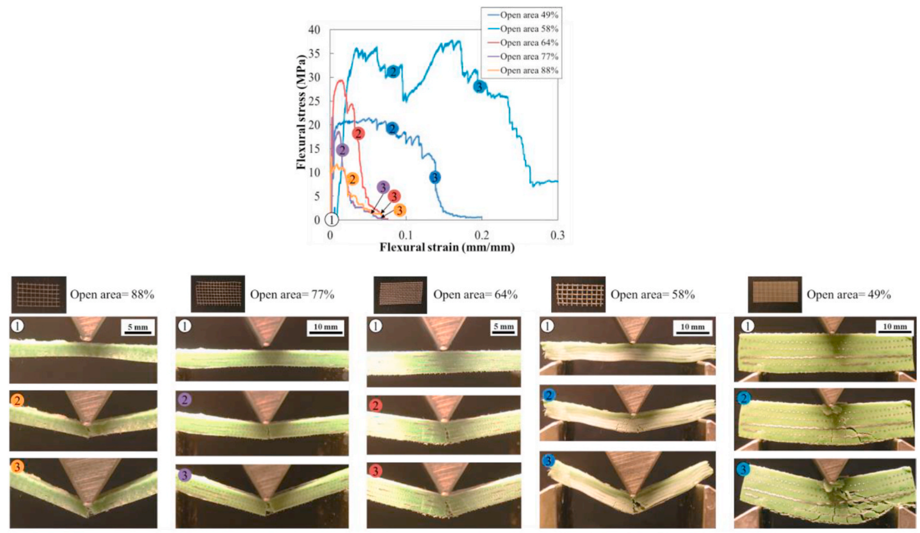

Fig. 8. a) Flexural stress-strain curves for the five multi-layered CS-Ti beams (five bilayers, 94.1%vol of CS); sequence of pictures of typical failure for samples prepared with b) 49% open area meshes, c) 58%, d) 64%, e) 77%, and f) 88%. The numbers 1, 2, 3 on the stress-strain curves indicate the time that each picture was taken.

taken during the tests (Fig. 8d–f) also showed a marked difference between these two groups of samples: The samples reinforced with Ti-mesh with open area of 48% and 59% revealed extensive crack deflection and multiple cracks within the same CS-layer. This mechanism gave rise to a diffuse damage zone roughly triangular in shape. In contrast, samples with higher open areas showed little crack deflection, with a single crack localized under the loading nose. The Ti-meshes were highly stretched across the cracks in these samples, but damages and large deformation were localized in a small volume, which explains the limited strain at failure in these samples. The samples fabricated with coarse meshes had an adhesion between CS and the Ti-mesh that was too high, preventing delamination and the spreading of damage. The absence of delamination significantly decreased mechanical performance, as predicted by the numerical models.

Fig. 9 shows the flexural modulus (initial slope on the stress-strain curve), the flexural strength (maximum flexural stress) and the toughness (defined as dissipated energy per unit volume (J/m^3) and computed from the area under the flexural stress-strain curve). Reinforced samples did not exhibit improvement in flexural modulus compared to plain CS. On the contrary, the imperfect Ti-CS interfaces decreased the stiffness of the material. Samples fabricated with 58% open area mesh were the most compliant (flexural modulus of 1.63 GPa, whereas CS has a stiffness of 18.58 GPa). Strength was however significantly higher ($p < 0.05$) for the 58% open area mesh than for the other types of mesh, reaching 34.86 MPa which suggests that this mesh was optimal. This represents an improvement of 9.5% on the strength of plain CS. Samples with higher open areas did not exhibited higher strength, possibly because of the lower strength of their interlayer according to the previous analytical investigation. The mesh with the smallest open area (49%) did not improve the strength of the material either. As discussed previously, this result can be attributed to a layer-interlayer interface toughness which is too low, but also to the stiffness of the interlayer, which was higher than that of the other interlayers (Fig. 6), a result that had been predicted by the FE analysis (Fracture scenarios l_1 and then l_1l_2 are promoted by low interlayer modulus). The most significant improvement in these materials was in terms of energy absorption (toughness), which was generated by crack bringing and plastic deformation in the Ti-meshes. Samples with 58% open area meshes showed the strongest evidence of bridging, with multiple loading peaks of the stress-strain curves, some of them higher than the initial peak. In these samples the toughness was about 100 times higher than plain CS, the greatest improvement among the five types of mesh.

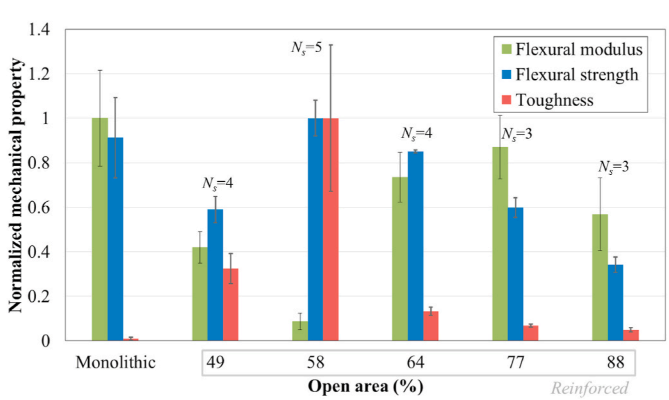

Fig. 9. Flexural strength, flexural stiffness, and energy dissipation (normalized by their largest values) of multi-layered CS-Ti beams prepared with Ti-meshes with five open areas (five bilayers, 94.1%vol CS) and a comparison with plain CS. N_s indicates the number of samples.

3.2. Effect of CS volume fraction

We now focus on designs based on Ti-mesh reinforcements with 58% open area, and we examine the effect of volume fraction of CS, controlled by keeping the number of bilayers at five and by adjusting the thickness of the CS layers. The total thicknesses of the multi-layered beams were therefore different for each CS volume fraction. We considered four volume fractions of CS: 94.1%vol, 90.5%vol, 84.1%vol, and 78%vol, with a minimum of three samples fabricated for each CS volume fraction. Fig. 10a shows typical flexural stress-strain curves that illustrate the effects of CS concentration and Fig. 10b shows snapshots of the samples fabricated with 90.5% and 78% vol. of CS at a flexural strain of 15%. The samples exhibited the same type of mechanical response, with extensive microcracking and Ti mesh deformation. The sample with 78% vol. CS however showed earlier debonding of the Ti mesh, with the result of a decrease strain at failure. Fig. 10c shows a summary of the mechanical performances (modulus, strength and toughness) as function of CS volume fraction. Because of the imperfect Ti-CS interfaces, the Young's modulus of the different composites tested here did not exceed about half of the stiffness of plain CS. The number of layers (and thus, the number of imperfect interfaces) was the same for all

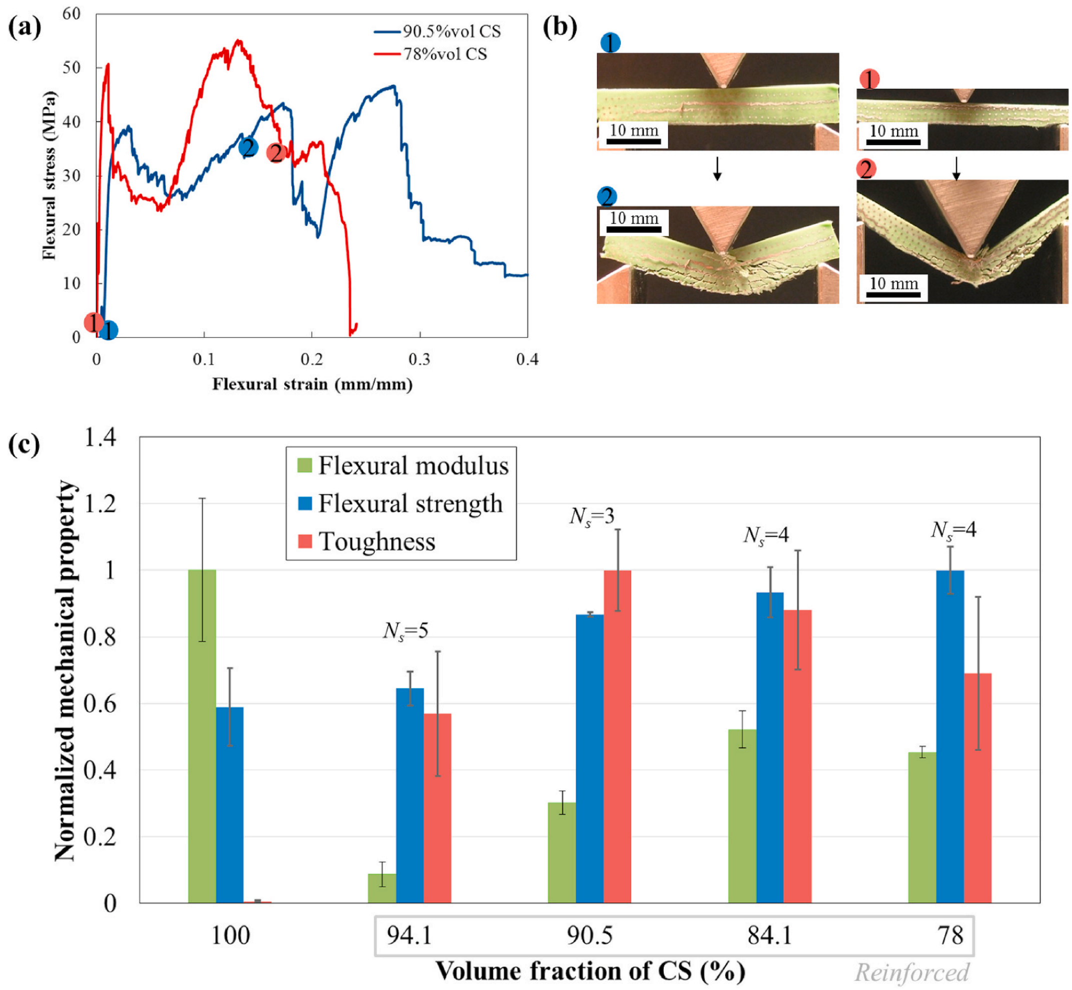

Fig. 10. a) Flexural stress-strain curves for two typical samples made with 90.5%vol and 78%vol of CS; b) pictures taken before and after failure of multi-layered beams made with 90.5%vol and 78%vol of CS (five bilayers, open area of 58%); c) mechanical properties (normalized by their largest value) of multi-layered CS-Ti beams prepared with four volume fractions of CS (five bilayers, open area of 58%) and a comparison with plain CS. N_s indicates the number of samples. Numbers 1 and 2 on the stress-strain curve indicate the time that each picture was taken.

samples. The increase in stiffness from 94.1 to 84.1% vol. CS sample can therefore be correlated with the change in volume fraction of Ti, since Ti has a higher tensile modulus (102–104 GPa (Niinomi, 1998) versus 18.58 GPa for CS). Strength also increased as the CS volume fraction decreased with a maximum attainted strength 70% higher than the strength of plain CS ($p < 0.05$, obtained with 78% vol. of CS). Lower CS volume fraction (i.e. higher fraction of Ti mesh) favored energy dissipation, but on the other hand samples with thin CS interfaces failed prematurely. These competing effects led to an optimal value 90.5% vol. CS for toughness.

3.3. Effect of number of layers

We now examine the effect of number of layers, with samples reinforced with the optimum Ti mesh (58% open area) and with the optimum CS concentration for toughness (90.5% vol). Different samples were fabricated with 3, 4, 5, 6 and 7 bilayers. A minimum of three samples were fabricated and tested for each number of layers. Fig. 11a shows two typical flexural stress-strain curves for samples with three and seven bilayers. The greater number of layers clearly offered more toughening mechanisms and delamination opportunities to propagating cracks. The associated pictures of sample failures in Fig. 11b indicates that the CS matrix cracked first while the Ti layers remained intact. The cracks then propagated at the Ti-CS interface as evidenced by the delamination of the layers on the picture. Such mechanism was a prediction of the numerical model and crucial element to improve the toughness of the composite. Moreover, additional fractures occurred on the bottom CS layers. This multiple cracking of the CS matrix was another mechanism that dissipated energy. For instance, with seven bilayers, the bottom CS layer was completely cracked when the initial crack reached the top CS layers, which resulted in a unique pyramid-like fracture pattern. Once the CS matrix was completely cracked and partially delaminated, other toughening mechanisms such as crack deflections or crack bridging took over and contributed again to the overall toughness. As a result, several peaks of various amplitudes (as exhibited on the stress-strain curves in Fig. 11a) were observed along the stress-strain curve until dramatic failure. Some peaks even presented an amplitude that was higher than the first peak, which explained the high toughness of the samples with a higher number of bilayers. Fig. 11c summarizes the effect of the number or bilayers on the Young's modulus, strength and toughness of the multi-layered beams. Overall, the Young's modulus of the samples decreased with higher number of layers, because of the larger number of imperfect Ti-CS interfaces. The strongest multi-layered sample (46.9 MPa) had 90.5%vol CS and $N = 5$ bilayers. This value represents an increase of 47% over plain CS. P-value calculations ($p > 0.05$) indicated that the $N = 5$, $N = 6$ and $N = 7$ data series were not statistically different which means that strength reached a plateau for $N > 5$. The reason could be the larger thickness and lower span-to-thickness ratio of these samples: studies (Garoushi et al., 2012; Alander et al., 2005) on composite materials have shown that decreasing

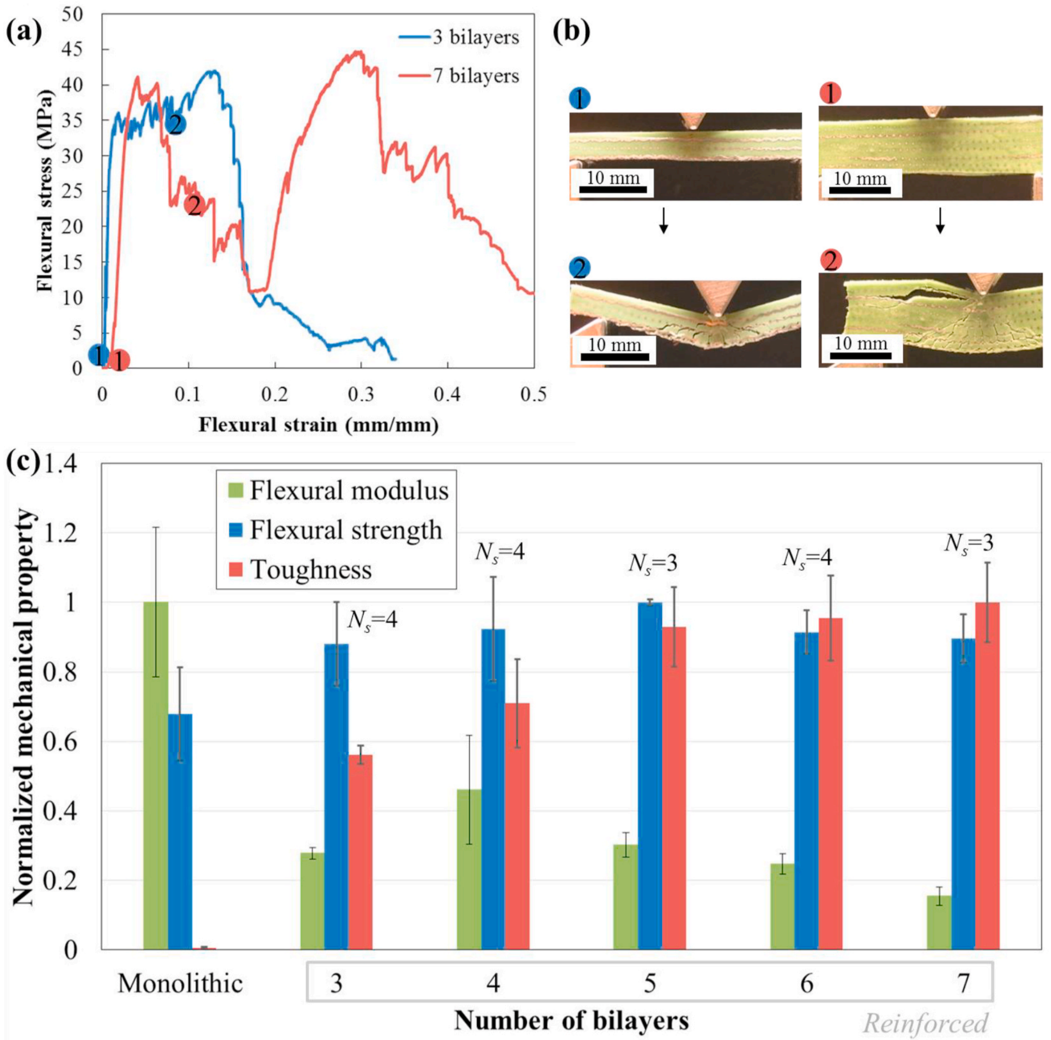

Fig. 11. a) Flexural stress-strain curves for two typical samples made with three and seven bilayers; b) pictures taken before and after failure of multi-layered beams made with three and seven bilayers (90.5%vol of CS, open area of 58%); c) mechanical properties (normalized by their largest value) of multi-layered CS-Ti beams prepared with three to seven bilayers (90.5%vol CS, open area of 58%) and a comparison with plain CS. N_s indicates the number of samples. Numbers 1 and 2 on the stress-strain curve indicate the time that each picture was taken.

the span-to-thickness ratio increases the shear stresses in the beam. These stresses become significant enough to affect flexural strength. In some cases, the maximum shear stress in the beam reaches the interface shear strength, and flexural strength is dramatically reduced (Daniel and Ishai, 1994). This effect, which was not taken into account in the analytical model, could have compensated for the increase in strength associated with larger N, resulting in a plateau for N > 5. Energy dissipation, however, increased continuously with N and was 195 times that of plain CS for N = 7. This result agrees with numerical and analytical models that indicated that higher values of N promote scenario l_1l_2.

4. Discussion

CS exhibits remarkable biodegradability and osteoconductivity and is therefore among the best materials for bone grafting purposes. Its lack of mechanical properties is however a major barrier to further development and clinical applications. In a previous study (Cavelier et al., 2020), we demonstrated that reducing the porosity of CS by compressing it during the setting phase was the key to strengthening the material. The optimized CS was however still brittle, and its mechanical behavior was far from that of natural bone. The present study has addressed the problem of material toughness. Previous experimental and analytical studies on multi-layered (Clegg et al., 1990; Clegg, 1992; Phillipps et al., 1993; Kovar et al., 1998; He et al., 1994) and ductile particle-reinforced ceramics (Krstic, 1983; Sigl et al., 1988; Evans, 1990; Campbell et al., 1990; Topoleski et al., 1992) demonstrated how this architecture can amplify toughness with no decrease in strength. The multilayered architecture with hard layers and ductile layers also plays a major role for toughening in cortical bone (Ritchie et al., 2009). The models we present here provide useful guidelines for the choice of these interfaces: The interface must be ductile, and it should have a high strength to stiffness ratio compared to the hard layers to ensure the proper sequence of failure. The models also indicated the importance of a large number of layers. We fabricated and tested a calcium sulfate-based multilayered material that embodies these design guidelines. We chose titanium as a biocompatible interface, with a woven mesh architecture to control the adhesion on CS. The experimental results confirmed the reinforcing potential of Ti on CS as predicted by the analytical model: different types of mesh provided various levels of interface-CS adhesion and stiffness, which were critical to mechanical performance. Meshes with larger open areas exhibited poor strength and toughness, which can be attributed to a layer-interlayer adhesion that was too high to provide moderate delamination. The mesh with the smallest open area was not optimal either, because of the higher stiffness of the interlayers, which was not advantageous as predicted by the numerical and analytical models. We found that the optimal mesh for strength and toughness was with 58% open area. Flexural modulus was however relatively low with this Ti mesh, probably because of a high CS-Ti interface compliance due to defects. The 58% open area mesh was selected for further investigation of the effect of volume fraction and number of bilayers. The Ti volume fraction positively affected both strength and toughness. Overall, the strongest and toughest samples were those prepared with 84.1%vol and 90.5%vol of CS. Finally, both the numerical and the analytical models predicted that the l_1 and l_1l_2 scenarios were promoted by large N (number of bilayers). This result was verified experimentally because toughness clearly increased with N. Strength, however, exhibited a more subtle correlation with increasing N: beams were stronger from $N = 3$ to $N = 5$, in agreement with both numerical and analytical investigations. Strength then saturated and reached a plateau around 45 MPa. Some crucial elements in the numerical analysis, such as CS matrix cracking or delaminations at the Ti-CS interfaces were observed in the experiments especially with a higher number of layers. As predicted by the models, Ti layers remained intact while CS layers fractured successively. While the initial crack propagated in the successive CS layers, the bottom CS layers fractured multiple times. At this point of the experiments, matrix cracking, crack deflection, delamination and crack bridging were all observed and a unique pyramid-like fracture pattern was revealed. These toughening mechanisms provoked peaks of high amplitude in the stress-strain curve and contributed to improve the mechanical properties of the composite.

5. Conclusion

This study was motivated by the lack of mechanical properties of calcium based bone graft materials despite their superior physical properties such as their osteoinductivity. To address this issue, we combined two biomaterials with dissimilar mechanical properties: Titanium and calcium sulfate. The major contribution of this study was to design and optimize a novel architecture via numerical analysis. The lessons of this analysis were the importance of both the brittle matrix (to dissipate energy through cracking) and the ductile layers (to deflect and bridge cracks, and dissipate energy through interlayer debonding). Materials were selected carefully to satisfy these conditions and prototypes were fabricated with CS and Ti. These prototypes were tested in three-point bending. Overall, the best material was achieved with a Ti-mesh with an open area of 58%, 90.5%vol of CS, and five bilayers: the toughening mechanisms predicted in the numerical analysis were prominent in this type of sample. As a result, the multi-layered Ti-CS samples with this multilayered design exhibited a toughness 180 times larger than that of plain CS, together with a 46% increase in strength. Further investigations on this multi-layered bone grafts will include testing in simulated body fluid and an in-vivo environment because the presence of Ti could affect both the degradation and the osteoconductivity of CS. It is also unknown how the mechanical properties of the implant will evolve while the graft is biodegrading: dissolution of CS could affect the adhesion of CS layers to the Ti-mesh and compromise the integrity of the composite graft. Ideally, the resorption of CS will match the regeneration of healthy bone to preserve its integrity, strength and toughness.

Author statement

Sacha Cavelier: Developed the analytical model, designed experiments, prepared samples, performed experiments, analyzed results, discussed results, prepared figures and wrote manuscript. Alireza Mirmohammadi: Developed the numerical model, prepared samples, performed experiments, analyzed results. François Barthelat: Supervision, technical and scientific advice, editing of the figures and manuscript.

Declaration of competing interest

The authors declare that there is no conflict of interest.

Acknowledgements

This work was supported by a grant from the Natural Sciences and Engineering Research Council of Canada and the Canadian Institutes of Health Research through a Collaborative Health Research Projects (CHRP). S.C. and A.M. were partially supported by a McGill Engineering Doctoral Award.

Appendix A. Supplementary data

Supplementary data to this article can be found online at https://doi.org/10.1016/j.jmbbm.2021.104461.

References

Ager, J.W., Balooch, G., Ritchie, R.O., 2006. Fracture, aging, and disease in bone. J. Mater. Res. 21, 1878–1892.
Alander, P., Lassila, L.V.J., Vallittu, P.K., 2005. The span length and cross-sectional design affect values of strength. Dent. Mater. 21, 347–353.
Anusavice, K.J., 2003. Phillips' Science of Dental Materials, eleventh ed. Saunders.
Azer, S.S., Kerby, R.E., Knobloch, L.A., 2008. Effect of mixing methods on the physical properties of dental stones. J. Dent. 36, 736–744.
Baino, F., 2017. Ceramics for bone replacement: commercial products and clinical use. In: Palmero FC, P., De Barra, E. (Eds.), Advances in Ceramic Biomaterials. Woodhead Publishing (Elsevier), Duxford (UK), pp. 249–278.
Barthelat, F., Rabiei, R., 2011. Toughness amplification in natural composites. J. Mech. Phys. Solid. 59, 829–840.
Barthelat, F., Tang, H., Zavattieri, P.D., Li, C.M., Espinosa, H.D., 2007. On the mechanics of mother-of-pearl: a key feature in the material hierarchical structure. J. Mech. Phys. Solid. 55, 306–337.
Bechtle, S., Habelitz, S., Klocke, A., Fett, T., Schneider, G.A., 2010. The fracture behaviour of dental enamel. Biomaterials 31, 375–384.
Bohner, M., 2010. Design of ceramic-based cements and putties for bone graft substitution. Eur. Cell. Mater. 20, 1–12.
Bohner, M., Galea, L., Doebelin, N., 2012. Calcium phosphate bone graft substitutes: failures and hopes. J. Eur. Ceram. Soc. 32, 2663–2671.
Budiansky, B., Hutchinson, J.W., Evans, A.G., 1986. Matrix fracture in fiber-reinforced ceramics. J. Mech. Phys. Solid. 34, 167–189.
Campbell, G.H., Ruhle, M., Dalgleish, B.J., Evans, A.G., 1990. Whisker toughening: a comparison between aluminum oxide and silicon nitride toughened with silicon carbide. J. Am. Ceram. Soc. 73, 521–530.
Cavelier, S., Dastjerdi, A.K., McKee, M.D., Barthelat, F., 2018. Bone toughness at the molecular scale: a model for fracture toughness using crosslinked osteopontin on synthetic and biogenic mineral substrates. Bone 110, 304–311.
Cavelier, S., Tanzer, M., Barthelat, F., 2020. Maximizing the strength of calcium sulfate for structural bone grafts. Journal of Bone Material Research, Part B 108, 963–971.
Chan, K.S., He, M.Y., Hutchinson, J.W., 1993. Cracking and stress redistribution in ceramic layered composites. Materials Science and Engineering a-Structural Materials Properties Microstructure and Processing 167, 57–64.
Clegg, W.J., 1992. The fabrication and failure of laminar ceramic composites. Acta Metall. Mater. 40, 3085–3093.
Clegg, W.J., Kendall, K., Alford, N.M., Button, T.W., Birchall, J.D., 1990. A simple way to make tough ceramics. Letters to Nature 347, 455–457.
Coetzee, A.S., 1980. Regeneration of bone in the presence of calcium sulfate. Arch. Otolaryngol. Head Neck Surg. 106, 405–409.
Coombes, A.G.A., Meikle, M.C., 1994. Resorbable synthetic polymers s replacements for bone graft. Clin. Mater. 17, 35–67.
Coutts, R.S.P., 1986. Wood-fibre reinforced plaster. J. Mater. Sci. 21, 2959–2964.
Craig, R.G., Powers, J.M.S.R.L., 2006. Craig's Restorative Dental Materials, twelfth ed. Mosby Elsevier, St. Louis, Mo.
Daniel, I.M., Ishai, O., 1994. Engineering Mechanics of Composite Materials. Oxford University Press, New York.
Donati, D., Zolezzi, C., Tomba, P., Vigano, A., 2007. Bone grafting: historical and conceptual review, starting with an old manuscript by Vittorio Putti. Acta Orthop. 78, 19–25.
Evans, A.G., 1990. Perspective on the development of high-toughness ceramics. J. Am. Ceram. Soc. 73, 187–206.
Evans, A.G., McMeeking, R.M., 1986. On the toughening of ceramics by strong reinforcements. Acta Metall. 34, 2435–2441.
Garoushi, S., Lassila, L.V.J., Vallittu, P.K., 2012. The effect of span length of flexural testing on properties of short fiber reinforced composite. J. Mater. Sci. Mater. Med. 23, 325–328.
Hahn, H., Palich, W., 1970. Preliminary evaluation of porous metal surfaced titanium for orthopedic implants. J. Biomed. Mater. Res. 4, 1–7.
Hall, M.J., DeFrances, C.J., Williams, S.N., Golosinskiy, A., Schwartzman, A., 2010. National hospital discharge survey: 2007 summary. In: Report NHS, pp. 1–20.

He, M.Y., Evans, A.G., Hutchinson, J.W., 1994. Crack deflection at an interface between dissimilar elastic materials: role of residual stresses. Int. J. Solid Struct. 31, 3443–3455.
Koester, K.J., Ager, J.W., Ritchie, R.O., 2008. The true toughness of human cortical bone measured with realistically short cracks. Nat. Mater. 7, 672–677.
Kovar, D., Thouless, M.D., Halloran, J.W., 1998. Crack deflection and propagation in layered silicon nitride/boron nitride ceramics. J. Am. Ceram. Soc. 81, 1004–1012.
Krstic, V.D., 1983. On the fracture of brittle-matrix ductile-particles composites. Philosophical Magazine a-Physics of Condensed Matter Structure Defects and Mechanical Properties 48, 695–708.
Kruger, R., Groll, J., 2012. Fiber reinforced calcium phosphate cements - on the way to degradable load bearing bone substitutes? Biomaterials 33, 5887–5900.
Kyung KH, Meyer C. Aramid fiber mesh as reinforcement of concrete panels subjected to high strain rates. 1st International RILEM Conference on Textile Reinforced Concrete2006.
LeGeros, R.Z., 2002. Properties of osteoconductive biomaterials: calcium phosphates. Clin. Orthop. Relat. Res. 81–98.
Li, V.C., Wang, Y.J., Backer, S., 1991. A micromechanical model of tension-softening and bridging toughening of short random fiber reinforced brittle matrix composites. J. Mech. Phys. Solid. 39, 607–625.
Maeda, S.T., Bramante, C.M., Taga, R., Garcia, R.B., de Moraes, I.G., Bernadineli, N., 2007. Evaluation of surgical cavities filled with three types of calcium sulfate. J. Appl. Oral Sci. 15, 416–419.
Mankin, H.J., 1987. Orthopedics in 1997 - advances and current problems. Journal of Bone and Joint Surgery-American 69A, 1257–1259.
McKee, J.C., Bailey, B.J., 1984. Calcium sulfate as a mandibular implant. Otolaryngology-Head Neck Surg. (Tokyo) 92, 277–286.
Moore, W.R., Graves, S.E., Bain, G.I., 2001. Synthetic bone graft substitutes. ANZ J. Surg. 71, 354–361.
Moreau, J.L., Weir, M.D., Xu, H.H., 2009. Self-setting collagen-calcium phosphate bone cement: mechanical and cellular properties. J. Biomed. Mater. Res. 91, 605–613.
Muller, M.A., Frank, A., Briel, M., Valderrabano, V., Vavken, P., Entezari, V., et al., 2013. Substitutes of structural and non-structural autologous bone grafts in hindfoot arthrodeses and osteotomies: a systematic review. BMC Muscoskel. Disord. 14.
Nalla, R.K., Kinney, J.H., Ritchie, R.O., 2003. Mechanistic fracture criteria for the failure of human cortical bone. Nat. Mater. 2, 164–168.
Nalla, R.K., Kruzic, J.J., Ritchie, R.O., 2004. On the origin of the toughness of mineralized tissue: microcracking or crack bridging? Bone 34, 790–798.
Nalla, R.K., Kruzic, J.J., Kinney, J.H., Ritchie, R.O., 2005. Mechanistic aspects of fracture and R-curve behavior in human cortical bone. Biomaterials 26, 217–231.
Niinomi, M., 1998. Mechanical properties of biomedical titanium alloys. Materials Science and Engineering a-Structural Materials Properties Microstructure and Processing 243, 231–236.
Noyama, Y., Miura, T., Ishimoto, T., Itaya, T., Niinomi, M., Nakano, T., 2012. Bone loss and reduced bone quality of the human femur after total hip arthroplasty under stress-shielding effects by titanium-based implant. Mater. Trans. 53, 565–570.
Phillipps, A.J., Clegg, W.J., Clyne, T.W., 1993. Fracture behaviour of ceramic laminates in bending—I. Modelling of crack propagation. Acta Metall. Mater. 41, 805–817.
Pietrzak, W.S., Ronk, R., 2000. Calcium sulfate bone void filler: a review and a look ahead. J. Craniofac. Surg. 11, 327–333.
Pneumaticos, S.G., Triantafyllopoulos, G.K., Basdra, E.K., Papavassiliou, A.G., 2010. Segmental bone defects: from cellular and molecular pathways to the development of novel biological treatments. J. Cell Mol. Med. 14, 2561–2569.
Ranjan, R., 2010. Fate of hydroxyapatite crystals used as bone graft substitute in benign lytic lesions of long bones. Internet J. Orthop. Surg. 18.
Ritchie, R.O., Buehler, M.J., Hansma, P., 2009. Plasticity and toughness in bone. Phys. Today 62, 41–47.
Saini, M., Singh, Y., Arora, P., Arora, V., Jain, K., 2015. Implant biomaterials: a comprehensive review. World Journal of Clinical Cases 3, 52–57.
Sigl, L.S., Mataga, P.A., Dalgleish, B.J., McMeeking, R.M., Evans, A.G., 1988. On the toughness of brittle materials reinforced with a ductile phase. Acta Metall. 36, 945–953.
Suchy, T., Balik, K., Cerny, M., Sochor, M., Hulejova, H., Pesakova, V., et al., 2008. A composite based on glass fibers and siloxane matrix as a bone replacement. Ceramics 52, 29–36.
Thouless, M.D., Evans, A.G., 1988. Effects of pull-out on the mechanical properties of ceramic-matrix composites. Acta Metall. 36, 517–522.
Thurner, P.J., Chen, C.G., Ionova-Martin, S., Sun, L.L., Harman, A., Porter, A., et al., 2010. Osteopontin deficiency increases bone fragility but preserves bone mass. Bone 46, 1564–1573.
Topoleski, L.D.T., Ducheyne, P., Cuckler, J.M., 1992. The fracture toughness of titanium fiber reinforced bone cement. J. Biomed. Mater. Res. 26, 1599–1617.
Turner, T.M., Urban, R.M., Gitelis, S., Haggard, W.O., Richelsoph, K., 2003. Resorption evaluation of a large bolus of calcium sulfate in a canine medullary defect. Orthopedics 26, S577–S579.
Weiner, S., Wagner, H.D., 1998. The material bone: structure mechanical function relations. Annu. Rev. Mater. Sci. 28, 271–298.
Xu, H.H.K., Quinn, J.B., 2002. Calcium phosphate cement containing resorbable fibers for short-term reinforcement and macroporosity. Biomaterials 23, 193–202.
Yao, Y.M., Wang, X.M., Aswani, K., Mobasher, B., 2017. Analytical procedures for design of strain softening and hardening cement composites. International Journal of Advances in Engineering Sciences and Applied Mathematics 9, 181–194.
Zamborsky, R., Svec, A., Bohac, M., Kilian, M., Kokavec, M., 2016. Infection in bone allograft transplants. Experimental and Clinical Transplantation 14, 484–490.
Zhang, Y.R., Du, W., Zhou, X.D., Yu, H.Y., 2014. Review of research on the mechanical properties of the human tooth. Int. J. Oral Sci. 6, 61–69.